Journal of Materials Chemistry C

Accepted Manuscript

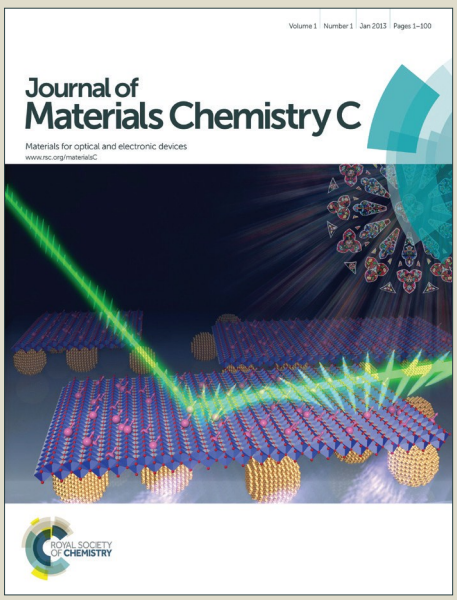

ROYAL SOCIETY OF CHEMISTRY

www.rsc.org/materialsC

Journal Name

ARTICLE TYPE

Cite this: DOI: 10.1039/xxxxxxxxxx

Silicon *de novo*: Energy filtering and enhanced thermoelectric performances of nanocrystalline silicon and silicon alloys

Dario Narducci,*[a] Stefano Frabboni,[b] and Xanthippi Zianni[c,d]

Received Date
Accepted Date

DOI: 10.1039/xxxxxxxxxx

www.rsc.org/journalname

Second-phase precipitation in nanocrystalline silicon may lead to improved thermoelectric power factors (up to ≈ 15 mW K^{-2}m^{-1} at room temperature) and high figures of merit. In this review energy filtering is shown to provide an explanatory framework for these findings, helping predict strategies to further improve nanocrystalline silicon efficiency in thermal harvesters.

1 Introduction

Silicon is the most widely used and better known functional material. It replaced germanium in microelectronics in the early 1960s[1] in spite of its lower carrier mobility. Silicon is also the reference material for photovoltaics, although it is an indirect–gap semiconductor. Also for thermoelectric (TE) applications silicon (alloyed with germanium) is the standard of the most mission–critical application, namely heat conversion in radioisotopic thermoelectric generators[2], although its TE efficiency is lower than that of other materials even at high temperatures. Apparently, silicon dominating role in many technological areas occurs *in spite of its intrinsic physical properties*. This cannot be solely related to its abundance and relatively low cost. One should actually note that silicon success is mostly due to its chemical and thermodynamic properties. The exceptional control level of its purity, the stability of its oxide, and the ease of doping has enabled an unsurpassed manufacturing control and extreme miniaturization. Also, silicon physical properties can be amply modified by playing with the physical chemistry of its impurities and defects. Thus, limited quantum efficiency in photovoltaic conversion compared to III-V semiconductors could be overcompensated by passivating Si extended defects e.g. with hydrogen[3]. And native low carrier mobility could be enhanced by delta–doping in stable Si–based nanostructures[4]. It would be then to no surprise to observe that the modest TE efficiency of silicon could also be improved by suitable chemical manipulations. In this review we will show how the TE performances of silicon (either bulk or thin films) could be actually improved over the last decade by taking advantage of its non–equilibrium solution chemistry. We will move from age-old evidence of anomalously high TE efficiencies observed in the Eighties, and rediscovered in recent years by a host of research groups worldwide. Such unexpected results are often explained as due to carrier energy filtering. However, enhanced TE efficiency is not ubiquitously found in silicon, so that the link between enhanced TE properties and the material microstructure remains unclear. Through a critical review of literature data we will show that high figures of merit cannot be simply explained as a result of carrier energy filtering at inter–grain barriers. Instead, improved TE efficiency requires the concurrency of carrier filtering and of a suitable microscopic temperature distribution within the material, resulting from the presence of a thermally insulating second phase segregating at grain boundaries. A semi–empirical model recently proposed by some of the present authors will be used to show how precipitates in silicon may be held responsible at one time for both the generation of potential barriers and for the local re–modulation of the temperature profile. Only when both effects occur does one observe an enhancement of the thermoelectric figure of merit. Data from the literature will provide a suitable benchmark of this interpretation.

2 Early observations of anomalies in degenerate nanocrystalline silicon

The TE properties of single–crystalline silicon were analyzed in the Fifties by Geballe and Hull[5], and recently re-measured by Stranz et al.[6]. Silicon has relatively high power factors $\sigma\alpha^2$ (where σ is the electrical conductivity and α is the Seebeck coefficient), especially at high carrier densities. However its relatively high thermal conductivity κ (≈ 120 W/mK at room temperature) keeps Si TE figure of merit $ZT = \sigma\alpha^2 T/\kappa$ (where T is the absolute temperature) from exceeding ≈ 0.01 at room temperature. In spite of its limited performances, still silicon has found appli-

[a] Dept. Materials Science, Univ. of Milano Bicocca, via R. Cozzi 55, 20125 Milano, Italy. Fax: +39 02 6448 5400; Tel: +39 02 6448-5137; E-mail: dario.narducci@unimib.it
[b] Dept. of FIM, Univ. of Modena and Reggio Emilia, via Campi 213/A, 41125 Modena, Italy.
[c] Dept. of Aircraft Technology, Technological Educational Inst. of Sterea Ellada, 34400 Psachna, Greece.
[d] Dept. of Microelectronics, INN, NCSR Demokritos, 15310 Athens, Greece.

cations in integrated microharvesters where its integrability has prevailed over its fair efficiency[7,8]. At the same time, strategies were explored to decrease its thermal conductivity without reducing the electrical conductivity. Among them, the use of SiGe alloys was rapidly found to be successful, improving TE efficiency up to $\approx 7\%$[2]. Germanium alloying favorably impacts on ZT by reducing the thermal conductivity while preserving σ through an increase of the carrier mobility μ. Raising ZT by decreasing κ is however in no way equivalent to do it by increasing the power factor (PF)[9]. Thus, other possibilities were suggested[10], including energy filtering and modulation doping. Instances of the latter were recently obtained in mixtures of two types of SiGe nanoparticles, one of which heavily doped[11], where a remarkable improvement of PF due to a mobility enhancement up to 50 % was reported for a $(Si_{95}Ge_5)_{0.65}(Si_{70}Ge_{30}P_3)_{0.35}$ mixture, leading to a $ZT \simeq 1.3$ at 900 °C.

Already in 1988 Vining anticipated that TE properties of boron–doped nanocrystalline silicon (ncSi) display an unexpected improvement upon prolonged annealing resulting in the precipitation of SiB_3[12], leading in turn to an unexpected increase of hole mobility when carrier density exceeds 10^{19} cm^{-3}[13]. Fig. 1 reports the Seebeck coefficient and the electrical conductivity measured in ncSi pellets obtained by hot–pressing at 1250 °C. Anomalies were observed in the two transport coefficients. The Seebeck coefficient was found to increase with the boron content between 1.0 % at. and 20 % at., a trend inconsistent with the expected decrease of α with increasing boron density. As SiB_3 precipitates had been detected, Vining conjectured that a second phase with larger α could be held responsible for the enhanced thermopower — although this could not explain carrier density data, getting to a maximum for a dopant concentration of 10 % at.. As of the hole mobility, anomalously high values were also obtained, ranging from 35 to 40 cm^{2}V^{-1}s^{-1} at 300 K. This finding was actually congruent with an early report by Seager[14] who had reported an increase of hole mobility 'approaching (within, say factors of 2 or 3) single–crystal values' in heavily boron–doped ncSi. Enhanced mobility was explained, according to Seto's model[15], as resulting from hole tunnelling at GB barriers, the width of which scales down with carrier density. Nonetheless, the role of boron segregation, as reported by Kamins[16], was left to be further clarified. Likely results were also reported by Loughin et al.[17] on B:SiGe alloys ($Si_{0.790}Ge_{0.197}B_{0.013}$). Upon annealing for 30 minutes at 1000 °C carrier density was found to decrease from 3.4×10^{20} to 3.1×10^{20} cm^{-3} with a ZT improvement of 12% that was also ascribed to the precipitation of a silicon boride from the solid solution.

3 Re-discovering nanocrystalline silicon as a thermoelectric material

As germanium alloying was accepted as the most reliable way to improve silicon TE efficiency, the unexpected increase of hole mobility in degenerate ncSi upon the formation of a SiB_x second phase was apparently not further considered or studied until recently. To the best of our knowledge we have actually to jump to 2008 to find again relevant reports on enhanced PFs in heav-

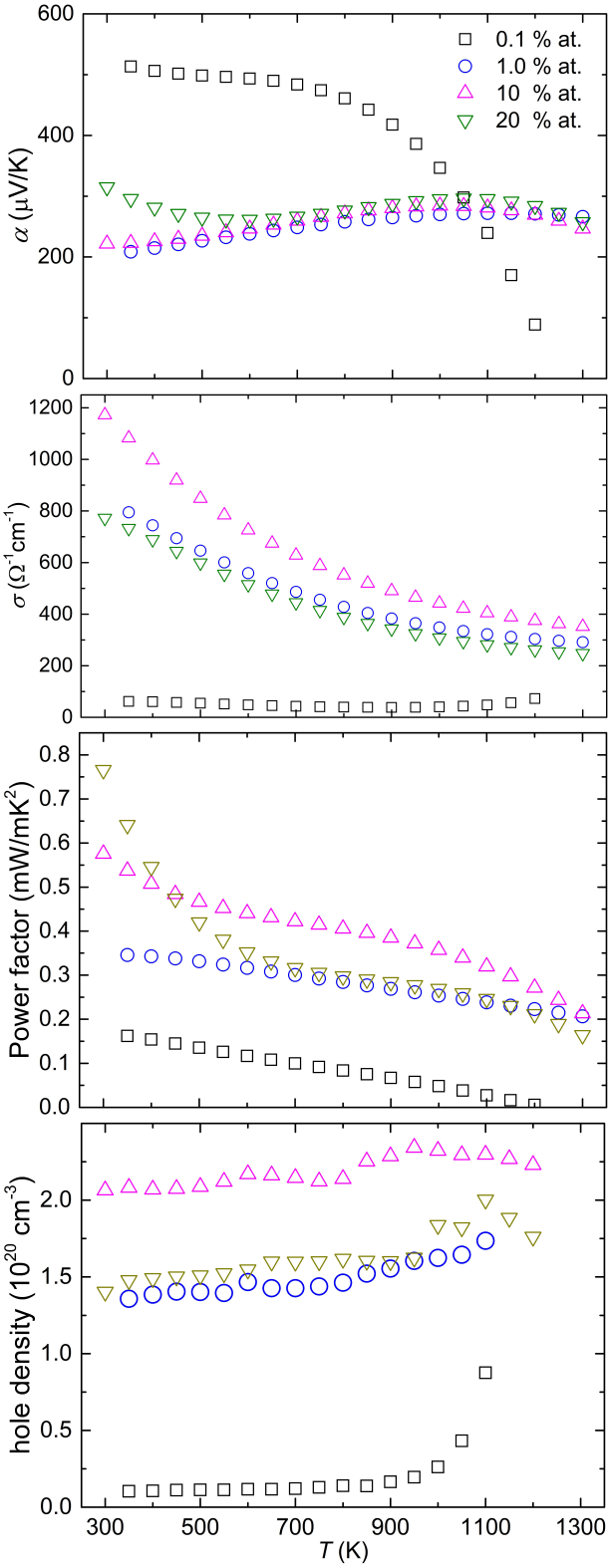

Fig. 1 Early evidence of anomalous thermoelectric trends in heavily doped hot–pressed ncSi samples: Seebeck coefficient, electrical conductivity, carrier density, and power factor as a function of temperature. Data from Ref. 13.

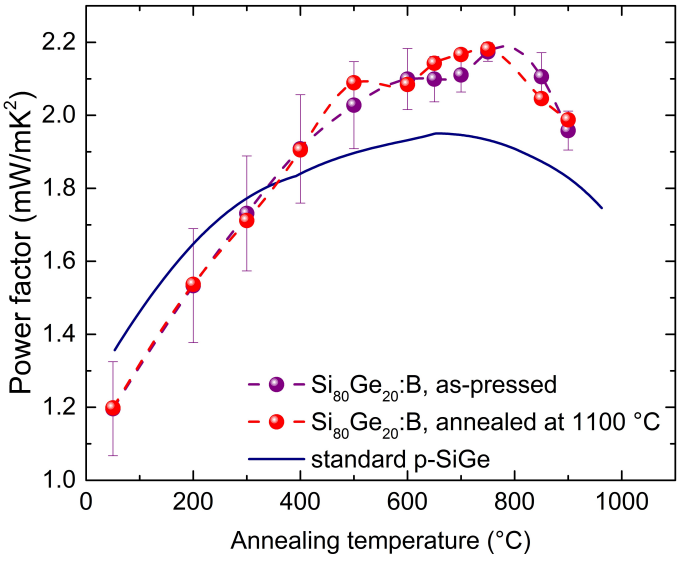

Fig. 2 Power factor of boron-doped $Si_{80}Ge_{20}$ pellets (as–pressed and after a 7–day annealing at 1100°C) compared to p-type SiGe bulk alloy. Dashed lines are eye–guides only. Data from Ref. 18.

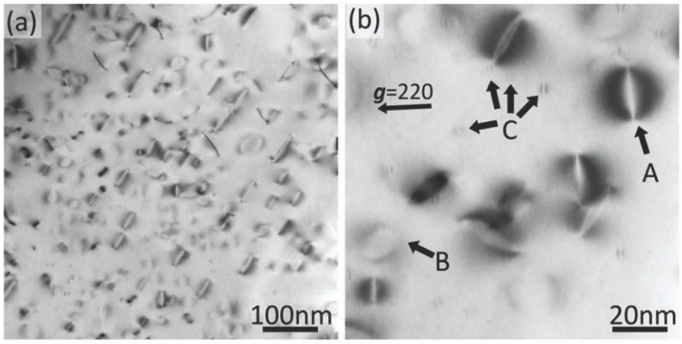

Fig. 3 Microstructure of a bulk $Si_{99}Ge_1P_3$ obtained by SPS. (a) Low- and (b) high-magnification TEM images show platelets of a second phase precipitated within the grain. Reproduced from Ref. 23 with permission from The Royal Society of Chemistry.

ily doped silicon. Dresselhaus and co-workers at MIT explored the effect of GBs on the σ/κ ratio in $Si_{0.80}Ge_{0.20}$ pressed powders with grain sizes between 5 and 50 nm and containing a large yet not quantified amount of boron. Pellets were found to display an increment of ZT up to 0.95 at 1000 °C[18,19]. Most of such improvement was actually due to a decrease of κ (by a factor 2 to 1.5 from 25 to 1000 °C). Nonetheless, also the PF underwent a small improvement of ≈ 15% at high temperature (up to 2.2 mW $K^{-2}m^{-1}$ at 800 °C) that was ascribed to the segregation of boron (Fig. 2). No improvement was instead found in P–doped pellets. Note that, in this as in all other cases of polycrystalline materials, PF values should not be directly compared to PFs in single-crystalline silicon as the thermal conductivity of single crystals is almost one order of magnitude larger than that of polycrystals. Likely investigations were carried out by Schierning and coworkers[20], who made however nanosilicon pellets using spark plasma sintering (SPS). They found a slightly larger improvement of the PF, up to 2.5 mW $K^{-2}m^{-1}$ at 700 °C after rapid thermal annealing at 1200 °C. Precipitation of silicon oxide was confirmed by x-ray analysis along with an increase of the carrier mobility that was anyway limited to 10 $cm^2V^{-1}s^{-1}$ at 300 K by the presence of grain boundaries. In a subsequent paper[21] the same collaboration provided transmission electron microscopy (TEM) evidence that sintering led to the precipitation of an amorphous phase. Power factors reached ≈ 4.5 mW $K^{-2}m^{-1}$ at 1000 °C in the best case, with a remarkable electron Hall mobility at room temperature of 61 $cm^2V^{-1}s^{-1}$.

The formation of a second phase was also explored in SiGe:B nanoparticles that were obtained by magnesioreduction starting from boron–doped silica and germania powders[22]. The detrimental role of grain boundaries limited however PFs to 1.3 mW $K^{-2}m^{-1}$.

Claims of high PFs (≈ 4.4 mW $K^{-2}m^{-1}$ at 800 °C) were also reported by Kurosaki and collaborators[23]. Nanometric precipitates of a phosphorus–rich second phase were observed in heavily phosphorus–doped Si and $Si_{99}Ge_1$ pellets obtained by SPS (Fig. 3). Structural (semi)coherence with the embedding microcrystalline silicon matrix led to a reduction of the thermal conductivity but also to an increase of the PF — both concurring to an increase of the ZT value.

The actual impact of dopant segregation on Si PF could be possibly better understood moving from pellets to thin films. Experimental evidence of a concurrent increase of the Seebeck coefficient and of the electrical conductivity in heavily boron–doped ncSi upon second phase precipitation was reported by Narducci et al.[24,25]. Thin silicon films doped with a boron concentration of 0.9 % mol. and with columnar nanograins having an in–plane size of ≈ 50 nm were annealed in one-hour isothermal cycles. Upon annealing, electrical conductivity initially decreased getting to a minimum at 800 °C, then increased up to almost double its as–deposited value. The Seebeck coefficient was instead observed to continually increase with the annealing temperature. As a result, PF reached the value of 13 mW $K^{-2}m^{-1}$ upon annealing at 1000 °C, with hole mobility at 300 K as large as 79 $cm^2V^{-1}s^{-1}$ [25,26] (Fig. 4). Further raising the nominal boron concentration and the annealing temperature resulted in PFs of 15.9 mW $K^{-2}m^{-1}$ and hole mobility of 145 $cm^2V^{-1}s^{-1}$ [27]. The dependence of the carrier density upon the annealing temperature suggested that the heat treatment had promoted the partial precipitation of boron in excess to its solid solubility[28]. Further analyses provided direct TEM evidence that 5–nm sized SiB_x second phase precipitated at grain boundaries[27] (Fig. 5).

Along the same line, Uchida and co-workers explored the thermoelectric properties of Si–$NiSi_2$ nanocomposites obtained by controlled phase segregation from thin films of metastable (amorphous) Ni–Si alloys doped with either boron or phosphorus[29]. A nanocomposite was obtained by rapid thermal annealing between 600 and 1200 °C. Formation of nanovoids decorating the grain boundaries was also observed, and was correlated to tensile strain at grain boundaries. The electrical conductivity decreased by annealing up to 800 °C, then increased for higher annealing temperatures. Seebeck coefficient showed instead a slight decrease (in absolute value) upon increasing the annealing temperature. As a result, the PF exceeded 1.9 mW $K^{-2}m^{-1}$ (p-type) and 1.1 mW

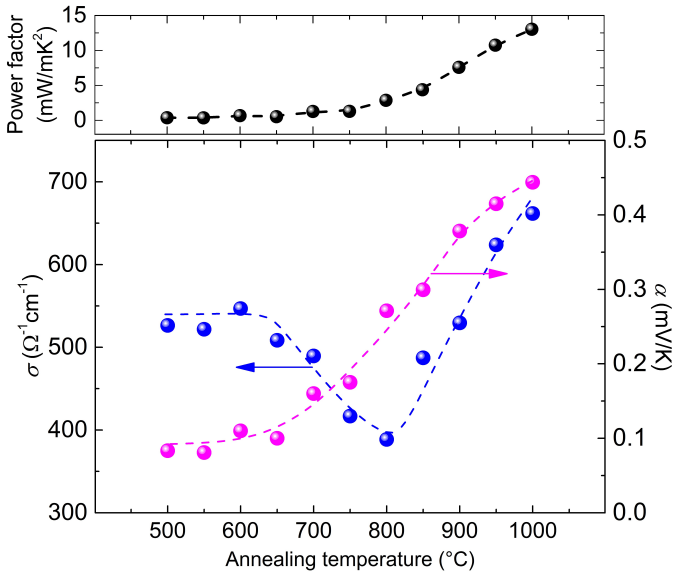

Fig. 4 Seebeck coefficient, electrical conductivity, and power factor at 300 K of heavily boron-doped nanocrystalline silicon thin films upon one-hour sequential annealing in argon. Data from Ref. 24.

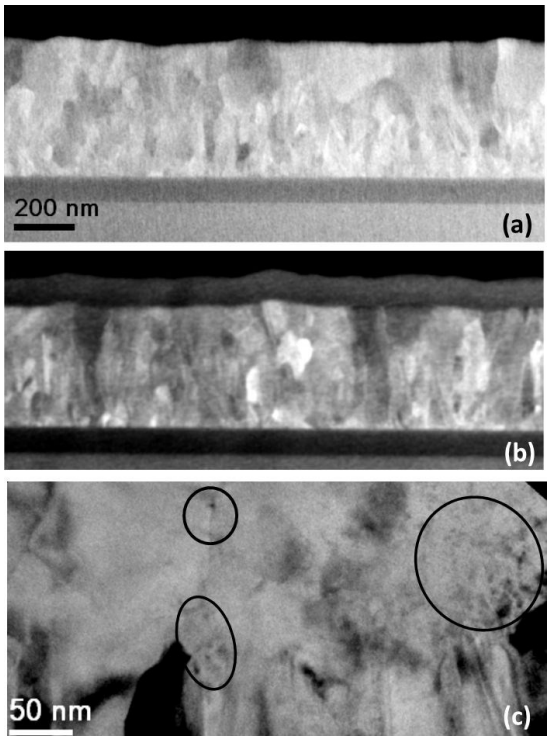

Fig. 5 (*a*) Dark field-STEM images of a heavily boron-doped ncSi film (*a*) as–deposited and (*b*) annealed at 1000°C. TEM bright field image (*c*) of the latter shows the occurrence of a second phase precipitated at GBs. Reproduced from Ref. 27 with permission from John Wiley & Sons.

$K^{-2}m^{-1}$ (n-type). Although these values were lower than those characterizing single-crystalline silicon at the same doping level, carrier mobility reached the value of 22 $cm^2V^{-1}s^{-1}$.

Table 1 summarizes a selection of morphological, compositional, and transport data in heavily-doped Si and Si–based nanocrystalline materials.

4 Energy filtering in composite semiconductors

The possibility of selecting carrier energies by the use of suitable potential barriers played a longstanding role in the physics of thermionic devices, entering the arena of thermoelectricity only in the Nineties through the pioneering work of Rowe and Min[30] who proposed the use of multiple potential barriers to enhance the Seebeck coefficient and the thermoelectric PF. While Shakouri *et al.* proposed the use of solid-state thermionics for thermoelectric applications[31], it was Mahan *et al.* who first suggested the use of multilayer thermionic emission to increase the TE efficiency[32,33]. Likely use of potential barriers to increase ZT through energy filtering was also advanced by Nishio and Hirano[34], who estimated the optimal barrier height and spacing using the Boltzmann Transport Equation (BTE). Large barriers and highly doped (degenerate) superlattices to increase the thermoelectric PF over bulk materials were also analyzed[35]. In perfect superlattices with planar boundaries, conservation of transverse momentum during thermionic emission limits the number of hot electrons emitted and the efficiency of solid-state thermionic energy conversion devices[36]. Yet, deviations from the perfect translational symmetry by non-planar boundaries, inhomogeneities (e.g. impurities), and dispersed nanoparticles[37,38] relax the condition for lateral momentum conservation and enhance the TE efficiency.

In a nutshell, energy filtering occurs when a potential barrier in an otherwise uniform medium prevents the diffusion/drift of carriers with energy E lower than the barrier height V_b (Fig. 6). Energy filtering causes a decrease of the density of carriers participating to transport and consequently a decrease of the electrical conductivity. Filtered carriers have however higher energies, so the Seebeck coefficient is enhanced. An overall increase of the PF is then possible if the Seebeck coefficient enhancement compensates for the decrease of the conductivity. Much theoretical investigation has been devoted on the prospects for PF enhancement by energy filtering using both simple and sophisticated models. The Seebeck coefficient enhancement by energy barriers in composite semiconductors has been explored using the non-equilibrium Green function method (NEGF) and a diffusion equation[39]. BTE has been also successfully used to interpret experimental data taking into account the relevant scattering mechanisms and additional scattering on energy barriers[40,41]. Analytical expressions for σ and α were obtained by Kajikawa[42–44] who applied an energy filtering model within BTE to polycrystalline semiconductors, assuming energy barriers of uniform heights. The model was then extended to examine the effect of barriers with fluctuating height[43]. Prospects for PF enhancement by energy barriers have been further explored recently using NEGF[45,46].

Table 1 Summary of transport properties of selected Si and Si-based heavily doped nanocrystalline materials. All transport data refer to 300 K unless otherwise stated.

Composition & preparation method	Doping $/10^{20}\mathrm{cm}^{-3}$	grain size /nm	σ $/\Omega^{-1}\mathrm{cm}^{-1}$	carrier density $/\mathrm{cm}^{-3}$	μ $/\mathrm{cm}^2\mathrm{V}^{-1}\mathrm{s}^{-1}$	α $/\mathrm{mV\ K}^{-1}$	PF $/\mathrm{mW\ K}^{-2}\ \mathrm{m}^{-1}$	Ref.
$Si_{80}Ge_{20}$:B, hot-pressed		5 – 50	850*			0.117*	1.16	18
$Si_{80}Ge_{20}$:B, hot-pressed		5 – 50	380†			0.25†	2.2†	18
$Si_{80}Ge_{20}$:P, hot-pressed	10.0	30 – 200	850*	2.2×10^{20}	10.3‡	−0.11*	1.0*	19
Si:B, SPS	5.0	44	230	3.8×10^{20}	2.9	0.17	0.5	20
Si:B, SPS	5.0	80	710	4.2×10^{20}	10.3	0.16	0.18	20
Si:B, SPS + HT 1000 °C	5.0	44	730	3.3×10^{20}	4.4	0.15	0.5	20
Si:B, SPS + HT 1000 °C	5.0	80	680	4.4×10^{20}	9.5	0.13	0.17	20
Si:P, SPS	5.0	42*	1075	1.1×10^{20}	61	−0.094	1.4	21
Si:P, SPS	15.0	5000	2520	3.84×10^{20}	43	−0.077	1.5‡	23
$Si_{99}Ge_1$:P, SPS	15.0	5000	2120	2.09×10^{20}	53	−0.087	1.6‡	23
$Si_{90}Ge_{10}$:B, hot-pressed	4.4	200	630‡	1.35×10^{20}	29	0.15	1.3	22
Si:B, CVD + II	4.4	50	550	2.6×10^{20}	13.3	0.08	0.35	24,25
Si:B, CVD + II + HT 1000 °C	4.4	50	670	5.6×10^{19}	79	0.44	13.0	24,25
Si:B, CVD + II + HT 1000 °C	6.0	75*	308	3.8×10^{19}	49	0.60	11.1	27
Si:B, CVD + II + HT 1070 °C	6.0	75*	256	1.1×10^{19}	145	0.79	15.9	27
Si–Ni:B, sputtering + HT 1200 °C	10.0	> 20	1200‡	3.4×10^{20}	22	0.13	1.9	29
Si–Ni:P, sputtering + HT 1200 °C	10.0	> 20	600‡	1.7×10^{20}	22	−0.15	1.1	29

* average value; † measured at 800 °C; ‡computed from reported data
HT = heat treatment; CVD = chemical vapour deposition; II = ion implantation

The ineffectiveness of the sole energy barriers to enhance thermoelectric efficiency has been rather extensively proved in the literature. Bachmann *et al.*[47] reached the conclusion that no improvement of the PF could be obtained because of the presence of potential barriers only. Using Seto's model[15] in a one-band effective mass approximation and within the Landauer formalism they investigated the influence of double Schottky barriers on the thermoelectric coefficients. Assuming that the double Schottky barriers arise due to trapping states at grain boundaries, electrostatic barriers were found to be too small to significantly impact on the thermoelectric parameters, independently of the doping level. Over the same period a BTE model was presented[41] to interpret the large PF enhancement observed in highly boron-doped nanocrystalline silicon[24,25,28]. It confirmed that the observed fivefold improvement of the PF cannot be interpreted solely by invoking electrostatic energy barriers at grain boundaries[41]. High PFs could be explained as the result of three factors, namely the presence of energy barriers at the grain boundaries due to the formation of a second-phase originating by boron segregation; the very high Fermi energy due to the high doping level; and a modification of the temperature landscape due to the formation of a low-κ second phase.

The parametric BTE model developed out of that analysis[48] may be conveniently used to provide a rationale for the whole set of data reported in Sect. 3. In the energy thermionic emission filtering model, the transmission probability $T(E)$ over a potential barrier of height V_b can be approximated by a step function:

$$T(E) = \begin{cases} 1 & E > V_\mathrm{b} \\ 0 & E < V_\mathrm{b} \end{cases} \tag{1}$$

For a bulk semiconductor and for $V_\mathrm{b} - E_\mathrm{F} \geq 2k_\mathrm{B}T$, analytical expressions for the conductivity σ_b and the Seebeck coefficient α_b

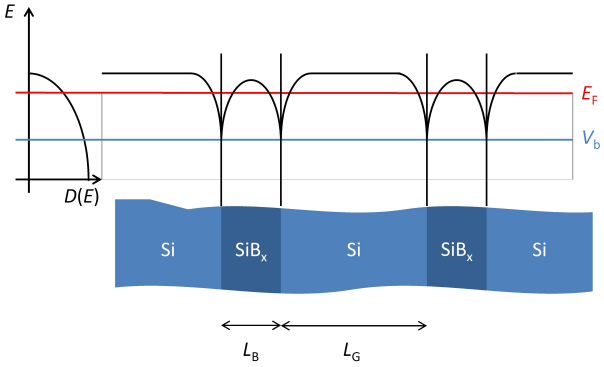

Fig. 6 Schematics of the energy filtering process in the ballistic regime for p-type nanocrystalline silicon. Low-velocity (low-energy) holes (dark gray) encounter a potential barrier at the Si–precipitate GB that prevents them from drifting/diffusing. Only may high-velocity carriers (light gray) pass the barrier. As a result, filtered carrier density no longer equals the (unfiltered) hole concentration.

in the presence of a barrier read

$$\sigma_\mathrm{b} = \sigma_\mathrm{C} F_p(x_\mathrm{b}) \tag{2}$$

and

$$\alpha_\mathrm{b} = -\frac{k_\mathrm{B}}{e}\left[\eta_\mathrm{F} - \left(p+\frac{5}{2}\right) - \Delta_p(x_\mathrm{b})\right] \tag{3}$$

where

$$\sigma_\mathrm{C} = \frac{4e^2}{3m^*} N_0 \tau_0 (k_\mathrm{B}T)^{p+\frac{3}{2}} \mathrm{e}^{\eta_\mathrm{F}} \Gamma\left(p+\frac{5}{2}\right) \tag{4}$$

with

$$F_p(x_\mathrm{b}) = 1 - \mathrm{e}^{-x_\mathrm{b}} x_\mathrm{b}^{p+\frac{5}{2}} \sum_{k=0}^{\infty} \frac{x_\mathrm{b}^k}{\Gamma\left(k+p+\frac{7}{2}\right)} \tag{5}$$

and

$$\Delta_p(x_\mathrm{b}) = \frac{\mathrm{e}^{-x_\mathrm{b}} x_\mathrm{b}^{p+\frac{5}{2}}}{\Gamma\left(p+\frac{5}{2}\right) F_p(x_\mathrm{b})} \tag{6}$$

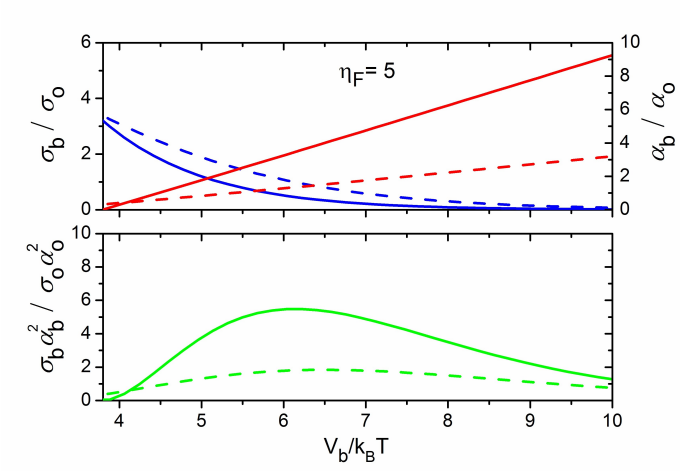

Fig. 7 The effect of an energy barrier on the transport coefficients. The conductivity is shown in blue, the Seebeck coefficient in red, and the PF in green. The solid (dashed) lines are for calculations using the analytical formalism for $p=-1/2$ ($p=3/2$). All coefficients are scaled with respect to the corresponding bulk values.

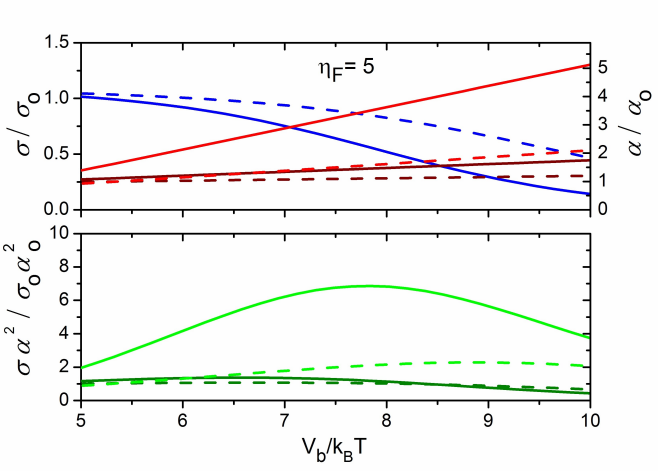

Fig. 8 The effect of energy barriers on the transport coefficients in the composite structure. The conductivity is shown in blue, the Seebeck coefficient in red, and the PF in green. Dark red and dark green are for a uniform thermal conductivity ($\kappa_B=\kappa_G$) while light red and light green are for $\kappa_B/\kappa_G=0.1$. The solid (dashed) lines are for calculations using the analytical formalism for $p=-1/2$ ($p=3/2$). All coefficients are scaled with respect to the corresponding bulk values.

In the above equations $\Gamma(z)$ is the gamma function, E_F is the Fermi level, and $\eta_F=E_F/k_BT$ and $x_b=V_b/k_BT$ are the reduce Fermi energy and barrier height.

Simplified expressions have been derived in Ref. 48 for the degenerate and non-degenerate transport regimes. In such formalism, common assumptions for the density of states $N(E)$ and the relaxation time τ have been used, namely that $N(E)=N_0E^r$ and $\tau(E)=\tau_0E^p$, where $r=1/2$ is for bulk one-band semiconductors and the exponent p characterizes the type of scattering, being $p=-1/2$ for phonon scattering and for highly screened ionized impurity scattering, and $p=3/2$ for ionized impurity scattering[49]. Typical dependency of σ, α, and the PF upon x_b compared to their values in the absence of a barrier are shown in Fig. 7. As expected, the conductivity decreases and the Seebeck coefficient increases with increasing barrier heights. Power factor enhancement is found at an optimal, intermediate barrier height.

This one-barrier regime dominates transport when the separation between barriers is smaller than the carrier mean free path (mfp) so that energy is not relaxed within the grains (ballistic regime)[39,45]. When the grain width is instead greater than the mfp, energy relaxation occurs within the grains (diffusive regime). In such a limit, energy barriers can be treated as independent and a network model can simulate the effective thermoelectric properties of the composite material assuming distinct properties within the grains and in the regions near the grain boundaries. The simplest model for such a composite would then consist of alternating grains and barrier regions. This model structure can be represented as a 1D network of resistors and voltage sources. Applying continuity of current and energy[39,45] gives the following expressions for the effective σ and α:

$$\frac{L}{\sigma}=\frac{L_G}{\sigma_G}+\frac{L_B}{\sigma_B} \tag{7}$$

$$\alpha=\frac{\alpha_G\dfrac{L_G}{\kappa_G}+\alpha_B\dfrac{L_B}{\kappa_B}}{\dfrac{L_G}{\kappa_G}+\dfrac{L_B}{\kappa_B}} \tag{8}$$

where L_G and L_B are the lengths of the grain (G) and barrier (B) regions, resp., and the subscripts label the pertinent transport coefficients. Their trends are displayed in Fig. 8, where the same values of E_F and p were used both in the grains and at the barrier region. Although more complex network model are surely needed to provide a more realistic representation of real polycrystalline composites, physics insights may be gained also within this simple 1D network model. Figure 8 shows how the effective conductivity keeps decreasing with increasing barrier height also in the effective medium. At the same time a small effective Seebeck enhancement (or no enhancement at all) is found when thermal conductivity is uniform (i.e. $\kappa_G=\kappa_B$). The Seebeck coefficient in the composite is instead significantly enhanced when the thermal conductivity is lower in the barrier region than within the grains. Thus, no PF enhancement is found in the composite for uniform thermal conductivity – in spite of the enhanced Seebeck coefficient in the barrier regions (Fig. 7). On the contrary, a remarkable PF enhancement is found when the thermal conductivity is non–uniform. And this may be actually the case of heavily doped ncSi, where precipitates at GBs may originate at one time a region of lower thermal conductivity (by enhanced phonon scattering in the presence of a second phase) and a potential barrier due to the formation of a Si–precipitate heterojunction.

5 Enhancement of silicon power factor by energy filtering

As already mentioned, formation of precipitates has been invoked with increasing frequency over the last years in several classes of thermoelectric materials to justify enhanced PFs[40,46,48,50]. How-

ever, only a few attempts of applying energy filtering theory to Si and Si-based systems have surfaced until now, and more effort in this direction might be encouraged. We have just shown how models predict that the formation of precipitates in ncSi may concur to filtering of carriers and to a favorable microscopic temperature distribution, leading to a remarkable increase of the PF that might reach values largely in excess of one around room temperature[41]. Specifically, and focusing initially on heavily boron-doped ncSi, the formation of SiB_x precipitates at GBs was shown to set conditions for energy filtering *sensu stricto* to occur; but it has also the non-marginal side effect of causing a distribution of the temperature drop across the material that privileges low-κ high-PF second phases, thereby leading to an additional increase of the PF[51]. On the experimental side a systematic study of the conditions actually leading to the anomalous increase of the PF in boron-doped ncSi proved that enhanced thermoelectric efficiency requires not only a boron concentration in excess to its solid solubility but also grain sizes smaller than ≈ 50 nm[27]. Apparently, for the mechanism to be effective in ncSi three conditions have to be satisfied:

(*a*) that the potential barrier height be such that the carrier density decrease enough to improve $|\alpha|$ but not so much that the increase of α be overcompensated by the decrease of σ;

(*b*) that the spacing between barriers be smaller than the mean free path of the relevant carrier (so preventing hot carrier thermalization) or the temperature distribution within the material (for $\kappa_{GB} \ll \kappa_B$) compensates for carrier thermalization (in the diffusive regime); and

(*c*) that second-phase precipitation occur at GBs.

Although the experimental analysis focused onto boron-doped ncSi, its results, along with the model reported in Sect. 4, may be used to provide a general rationale for the conditions to be fulfilled to enhance PF by energy filtering.

Condition (*a*) may be theoretically explained by inspecting Fig. 6. The barrier height obviously plays a critical role in energy filtering. Manifestly enough, for vanishing barrier heights no energy filtering may occur. Instead, exceedingly high barriers cut off a too large fraction of majority carriers, so that the enhancement of the average relaxation time cannot compensate for the decrease of carrier density. Therefore, while the Seebeck coefficient increases, the electrical conductivity drops down – and the material acts as a semi–insulator. Thus, an optimal value of V_b exists, that may be predicted using computational models[48] but that may also be searched for through a guided trial–and–error approach. Actually, since V_b scales with the Fermi energies of the two phases and with the density of interface trap states, scanning over total dopant concentration and over carrier density may provide an empirical way to optimize V_b[27,41].

Spacing between barriers (condition (*b*)) rules the carrier transport regime. Since energy filtering is mostly effective when majority carriers travel in a quasi–ballistic regime[46], the distance between pairs of barriers should not exceed the carrier mean free path. If this condition is not met, relaxation (thermalization) upon scattering rapidly washes out the beneficial effect of carrier filtering, holes (electrons) tending to recover their quasi–equilibrium distribution.

Also in this case, optimal spacing may be either computed[48] or experimentally evaluated by changing the size of the precipitates and/or the ncSi grain size. The two quantities are actually correlated in view of clause (*c*), stressing the importance that precipitation occur at GBs. It may be interesting to note that the relevance of precipitates decorating GBs was indirectly anticipated by Minnich[52] in SiGe nanocomposites. Minnich found that the GB potentials required to fit experimental data had to be set to values largely exceeding theoretical values computed in defect-free GBs. Among the possible explanations, the effect of a variety of nanoprecipitates at GBs acting as scattering sites had then to be set forth.

It should be stressed that precipitates may further modulate the macroscopic thermopower both in the ballistic and in the diffusive regimes. As mentioned, the eventual difference of thermal conductivities between silicon and the second phase partitions the applied temperature difference between silicon grains and the precipitates. Second phases with lower κ but higher α than silicon further enhance the effective (macroscopic) thermovoltage[39,45,46,53]. Thus, although this mechanism is not directly related to energy filtering, it actually strongly affects the observed PF, hiding or making more evident the occurrence of carrier screening at GB potential barriers.

If one accounts for the whole set of requirements, it may be not that striking the modest improvement of PFs in some ncSi pellets or thin films or the seeming inconsistency among reports concerning formally similar systems. Large grain sizes enable hot carrier relaxation, so that the equilibrium carrier energy distribution is recovered and filtering becomes macroscopically ineffective. Focusing onto ncSi, Table 1 shows how the largest PF are always observed when carrier mobility is high[21]. In turn, large mobility apparently occurs only when the actual carrier density is significantly lower than the nominal doping level, i.e. when the precipitation of a second phase is promoted either by SPS in pellets or by annealing in thin films.

Precipitates are however a necessary but not a sufficient condition to enhance the TE efficiency. Incoherent, discontinuous, or amorphized GBs may cause barriers to exceed the optimal height (thus violating clause (*a*)). Thus, an excessive reduction of the carrier density or, for very high barriers, a drop of the mobility easily explains the lack of PF improvement. As an extreme example, nanosilicon pellets (grain size ≈ 50 nm) of both n-($Si_{0.9640}P_{0.0288}Ga_{0.0072}$) and p-type ($Si_{0.980}B_{0.020}$), while displaying a major reduction of the thermal conductivity, showed no PF improvements[54]. Actually, n-type samples showed a reduction by 30 % of their electrical conductivity and p-type pellets reported an even larger decrease[55]. Occurrence (or at least effectiveness) of energy filtering had then to be ruled out[54] as a result of *gray* (i.e. non–energy dependent) carrier scattering at grain boundaries. Stated differently, exceedingly high barriers overkill the density of unfiltered carriers – so condition (*a*) is apparently not fulfilled. This might also explain the relatively low values of PF and carrier mobility observed in Si–$NiSi_2$ thin films where strain generated voids at GBs[29].

The same reasoning also help explain the results of Kurosaki's work[23], where a large PF improvement was obtained in *micro*crystalline pellets. Kurosaki actually showed that a high density of nanometric precipitates was found within the bulk of the grains. Thus, micrometric grains are actually nanocomposited themselves, with coherent crystallographic domains estimated around a few hundred nanometres, a size actually consistent with clauses (*b*) and (*c*).

6 Conclusions and Outlook

In this review we have discussed evidence from literature concerning the possibility of improving Si *ZT* by increasing its PF in nanocrystalline materials, where κ values are already at least one order of magnitude lower than in single crystals. Based upon literature data and models we have shown that energy filtering cannot be invoked as the sole factor leading to increased PFs. This help explain the apparent inconsistency among materials with similar doping levels and morphology. Consistently with a wealth of theoretical analyses, no significant improvement of the PF may occur only because of the presence of potential barriers within the material. Instead, precipitates have to play a twofold role, namely setting the potential barrier that filters out carriers and generating a temperature distribution within the composite that conveniently partitions the applied temperature difference, making it drop preferentially on the high-α phase. Bearing this in mind, all the experimental data available may be semi–quantitatively explained. Thus, from an experimentalist's point of view the most relevant issue to improve PF in Si remains that of controlling the mechanism of precipitation, so to have a high–α low–κ second phase forming at the matrix grain boundaries. For the most common silicon dopants, high solubility along with relatively small diffusivity implies long, high-temperature treatments that often may cause the concurrent increase of the grain size. As a result, the system may shift from the ballistic to the diffusive regime, and hot carriers may relax while drifting across grains with no compensation due to temperature redistribution (cf. clause (*b*). In addition, large densities of precipitates induce lattice strain that may reshape the electronic structure of silicon, with an eventual adverse contribution to the PF[56].

In summary, the body of evidence accumulated over the last few years apparently points out that energy filtering due to precipitates at grain boundaries *may* play a remarkable role in enhancing the PF of highly doped ncSi. However, stringent conditions on grain size and on thermal conductivity and Seebeck coefficient of the second phase must be met. With a thermal conductivity ranging from 25 down to 8 W $K^{-1}m^{-1}$ in a material that may be naturally integrated with standard electronics, the prospective of coupling higher PFs (and then higher TE efficiencies) with low costs and a large geo-abundance will surely drive further research over the next years — an effort that will also return an additional understanding of the intriguing physics and chemistry of nanocrystalline silicon.

Notes and references

1 J. T. Clemens, *Bell Labs Tech. J.*, 1997, **2**, 76–102.

2 J. Yang and T. Caillat, *MRS Bull.*, 2006, **31**, 224–229.

3 M. A. Green, *Prog. Photovoltaics Res. Appl.*, 2005, **13**, 447–455.

4 F. Schaffler, *Semicond. Sci. Technol.*, 1997, **12**, 1515–1549.

5 T. H. Geballe and G. W. Hull, *Phys. Rev.*, 1955, **98**, 940.

6 A. Stranz, J. Kaehler, A. Waag and E. Peiner, *J. Electron. Mater.*, 2013, **42**, 2381–2387.

7 M. Strasser, R. Aigner, M. Franosch and G. Wachutka, *Sens. Actuators, A*, 2002, **97 - 98**, 535 – 542.

8 Z. Yuan, K. Ziouche, Z. Bougrioua, P. Lejeune, T. Lasri and D. Leclercq, *Sens. Actuators, A*, 2015, **221**, 67 – 76.

9 D. Narducci, *Appl. Phys. Lett.*, 2011, **99**, 102104.

10 M. S. Dresselhaus, G. Chen, Z. Ren, J.-P. Fleurial, P. Gogna, M. Y. Tang, D. Vashaee, H. Lee, X. Wang, G. Joshi, G. Zhu, D. Wang, R. Blair, S. Bux and R. Kaner, MRS Proc., vol. 1044, 2007, pp. 1044–U02–04.

11 B. Yu, M. Zebarjadi, H. Wang, K. Lukas, H. Wang, D. Wang, C. Opeil, M. Dresselhaus, G. Chen and Z. Ren, *Nano Lett.*, 2012, **12**, 2077–2082.

12 C. B. Vining, *The Thermoelectric Properties of Boron-Doped Silicon and Silicon-Germanium in the As-Hot Pressed Conditions*, JPL/Calif. Inst. of Tech. technical report, 1988.

13 C. B. Vining, W. Laskow, J. O. Hanson, R. R. Van der Beck and P. D. Gorsuch, *J. Appl. Phys.*, 1991, **69**, 4333–4340.

14 C. H. Seager, *Annu. Rev. Mater. Sci.*, 1985, **15**, 271–302.

15 J. Y. W. Seto, *J. Appl. Phys.*, 1975, **46**, 5247–5254.

16 T. I. Kamins, *J. Appl. Phys.*, 1971, **42**, 4357–4365.

17 S. Loughin, D. X. Centurioni, A. G. Robison, J. J. Maley and J. P. Fleurial, *AIP Conf. Proc.*, 1993, **271**, 747 — 752.

18 G. Joshi, H. Lee, Y. Lan, X. Wang, G. Zhu, D. Wang, R. W. Gould, D. C. Cuff, M. Y. Tang, M. S. Dresselhaus, G. Chen and Z. Ren, *Nano Lett.*, 2008, **8**, 4670–4674.

19 X. W. Wang, H. Lee, Y. C. Lan, G. H. Zhu, G. Joshi, D. Z. Wang, J. Yang, A. J. Muto, M. Y. Tang, J. Klatsky, S. Song, M. S. Dresselhaus, G. Chen and Z. F. Ren, *Appl. Phys. Lett.*, 2008, **93**, 193121.

20 V. Kessler, D. Gautam, T. Huelser, M. Spree, R. Theissmann, M. Winterer, H. Wiggers, G. Schierning and R. Schmechel, *Adv. Energ. Mater.*, 2013, **15**, 379–385.

21 T. Claudio, N. Stein, D. G. Stroppa, B. Klobes, M. M. Koza, P. Kudejova, N. Petermann, H. Wiggers, G. Schierning and R. P. Hermann, *Phys. Chem. Chem. Phys.*, 2014, **16**, 25701–25709.

22 M. L. Snedaker, Y. Zhang, C. S. Birkel, H. Wang, T. Day, Y. Shi, X. Ji, S. Kraemer, C. E. Mills, A. Moosazadeh, M. Moskovits, G. J. Snyder and G. D. Stucky, *Chem. Mater.*, 2013, **25**, 4867–4873.

23 A. Yusufu, K. Kurosaki, Y. Miyazaki, M. Ishimaru, A. Kosuga, Y. Ohishi, H. Muta and S. Yamanaka, *Nanoscale*, 2014, **6**, 13921–13927.

24 D. Narducci, E. Selezneva, G. Cerofolini, E. Romano, R. Tonini and G. Ottaviani, 8th European Conf. on Thermoelectrics, 2010, pp. 141–146.

25 D. Narducci, E. Selezneva, G. Cerofolini, S. Frabboni and G. Ottaviani, *J. Solid State Chem.*, 2012, **193**, 19–25.

26 D. Narducci, E. Selezneva, G. Cerofolini, S. Frabboni and G. Ottaviani, *AIP Conf. Proc.*, 2012, **1449**, 311–314.

27 D. Narducci, B. Lorenzi, X. Zianni, N. Neophytou, S. Frabboni, G. C. Gazzadi, A. Roncaglia and F. Suriano, *Phys. Status Solidi A*, 2014, **211**, 1255–1258.

28 D. Narducci, E. Selezneva, A. Arcari, G. Cerofolini, E. Romano, R. Tonini and G. Ottaviani, MRS Proc., vol. 1314, 2011, pp. mrsf10–1314–ll05–16.

29 N. Uchida, T. Tada, Y. Ohishi, Y. Miyazaki, K. Kurosaki and S. Yamanaka, *J. Appl. Phys.*, 2013, **114**, 134311.

30 D. M. Rowe and G. Min, *AIP Conf. Proc.*, 1994, **316**, 339–342.

31 A. Shakouri and J. E. Bowers, *Appl. Phys. Lett.*, 1997, **71**, 1234–1236.

32 G. D. Mahan and L. M. Woods, *Phys. Rev. Lett.*, 1998, **80**, 4016–4019.

33 G. D. Mahan, J. O. Sofo and M. Bartkowiak, *J. Appl. Phys.*, 1998, **83**, 4683–4689.

34 Y. Nishio and T. Hirano, *Jap. J. Appl. Phys. Part 1*, 1997, **36**, 170–174.

35 A. Shakouri, C. LaBounty, P. Abraham, J. Piprek and J. E. Bowers, MRS Proc., vol. 545, 1998, p. 449.

36 D. Vashaee and A. Shakouri, *Phys. Rev. Lett.*, 2004, **92**, 106103.

37 J.-H. Bahk, Z. Bian and A. Shakouri, *Phys. Rev. B*, 2013, **87**, 075204.

38 S. V. Faleev and F. Léonard, *Phys. Rev. B*, 2008, **77**, 214304.

39 R. Kim and M. S. Lundstrom, *J. Appl. Phys.*, 2011, **110**, 034511.

40 A. Popescu, L. M. Woods, J. Martin and G. S. Nolas, *Phys. Rev. B*, 2009, **79**, 205302.

41 N. Neophytou, X. Zianni, H. Kosina, S. Frabboni, B. Lorenzi and D. Narducci, *Nanotechnology*, 2013, **24**, 205402.

42 Y. Kajikawa, *J. Appl. Phys.*, 2012, **112**, 123713.

43 Y. Kajikawa, *J. Appl. Phys.*, 2013, **114**, 053707.

44 Y. Kajikawa, *J. Appl. Phys.*, 2013, **114**, 043719.

45 R. Kim and M. S. Lundstrom, *J. Appl. Phys.*, 2012, **111**, 024508.

46 N. Neophytou and H. Kosina, *J. Appl. Phys.*, 2013, **114**, 044315.

47 M. Bachmann, M. Czerner and C. Heiliger, *Phys. Rev. B*, 2012, **86**, 115320.

48 X. Zianni and D. Narducci, *J. Appl. Phys.*, 2015, **117**, 035102.

49 M. Lundstrom, *Fundamentals of Carrier Transport*, Cambridge University Press, 2000.

50 N. Neophytou, *Eur. Phys. J. B*, 2015, **88**, 86.

51 N. Neophytou, X. Zianni, H. Kosina, S. Frabboni, B. Lorenzi and D. Narducci, *J. Electron. Mater.*, 2014, **43**, 1896–1904.

52 A. J. Minnich, H. Lee, X. W. Wang, G. Joshi, M. S. Dresselhaus, Z. F. Ren, G. Chen and D. Vashaee, *Phys. Rev. B*, 2009, **80**, 155327.

53 X. Zianni, N. Neophytou and D. Narducci, *Mater. Today: Proc.*, 2015, **2**, 497 – 503.

54 M. Zebarjadi, G. Joshi, G. Zhu, B. Yu, A. Minnich, Y. Lan, X. Wang, M. Dresselhaus, Z. Ren and G. Chen, *Nano Lett.*, 2011, **11**, 2225–2230.

55 S. Bux, J.-P. Fleurial, R. Blair, P. Gogna, T. Caillat and R. Kaner, MRS Proc., vol. 1166, 2009, pp. 1166–N02–04.

56 N. F. Hinsche, I. Mertig and P. Zahn, *J. Phys.: Condens. Matter*, 2011, **23**, 295502.

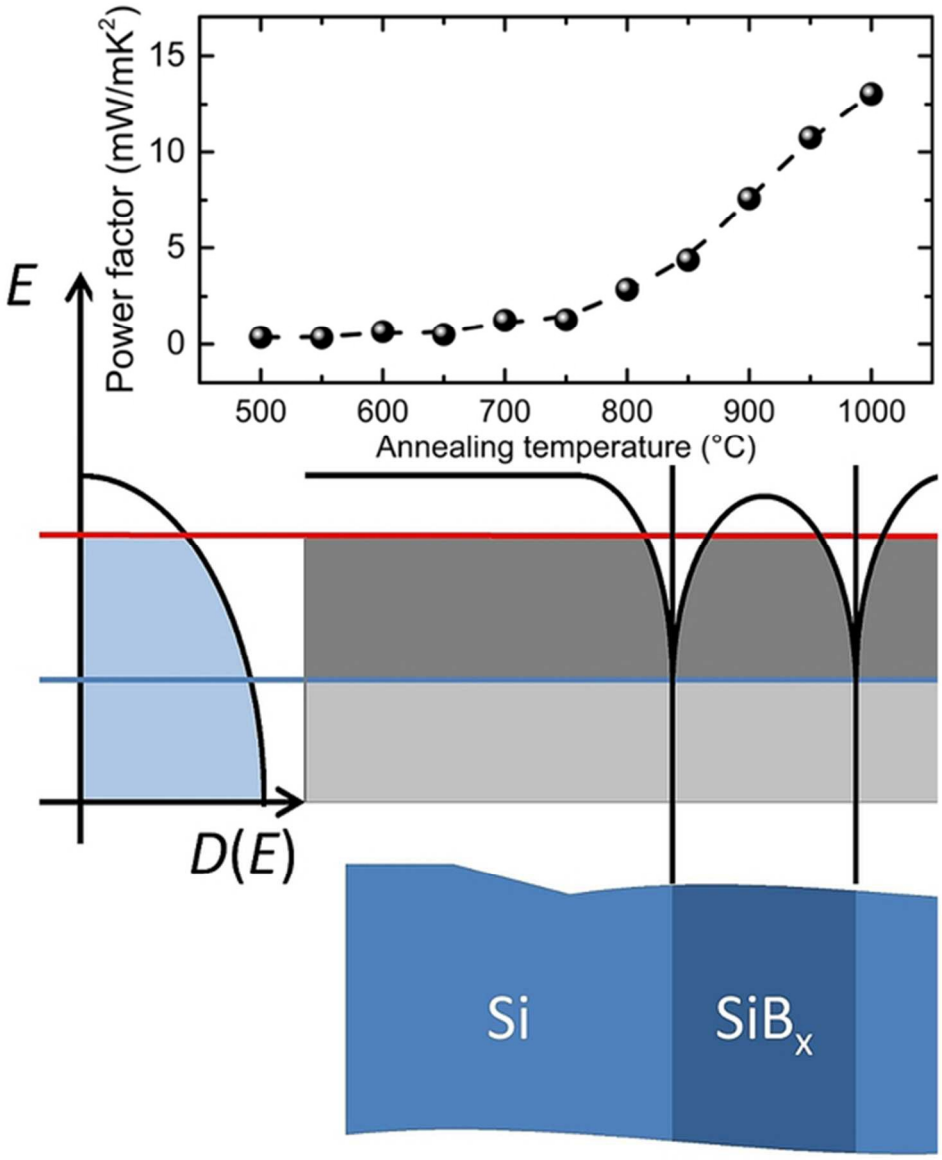

Energy filtering due to second-phase precipitation in nanocrystalline silicon may lead to remarkable improvements of its thermoelectric power factor.
49x62mm (300 x 300 DPI)